nature cell biology

LETTERS

Long-range self-organization of cytoskeletal myosin II filament stacks

Shiqiong Hu[1], Kinjal Dasbiswas[2,3], Zhenhuan Guo[1], Yee-Han Tee[1], Visalatchi Thiagarajan[1], Pascal Hersen[1,4], Teng-Leong Chew[5], Samuel A. Safran[2], Ronen Zaidel-Bar[1,7] and Alexander D. Bershadsky[1,6,7]

Although myosin II filaments are known to exist in non-muscle cells[1,2], their dynamics and organization are incompletely understood. Here, we combined structured illumination microscopy with pharmacological and genetic perturbations, to study the process of actomyosin cytoskeleton self-organization into arcs and stress fibres. A striking feature of the myosin II filament organization was their 'registered' alignment into stacks, spanning up to several micrometres in the direction orthogonal to the parallel actin bundles. While turnover of individual myosin II filaments was fast (characteristic half-life time 60 s) and independent of actin filament turnover, the process of stack formation lasted a longer time (in the range of several minutes) and required myosin II contractility, as well as actin filament assembly/disassembly and crosslinking (dependent on formin Fmnl3, cofilin1 and α-actinin-4). Furthermore, myosin filament stack formation involved long-range movements of individual myosin filaments towards each other suggesting the existence of attractive forces between myosin II filaments. These forces, possibly transmitted via mechanical deformations of the intervening actin filament network, may in turn remodel the actomyosin cytoskeleton and drive its self-organization.

Bundles of actin filaments also known as 'actin cables' or 'stress fibres' were found in non-muscle cells more than 40 years ago[3]. Soon after, it was shown that myosin (myosin II) forms periodic 'striations' along these bundles[4] while α-actinin forms striations[5] that are localized in the spaces between myosin striations[1,6]. The presence of myosin II filaments in non-muscle cells was unequivocally proved using electron microscopy of platinum replicas[2,7]. In these seminal papers, it was demonstrated that myosin II filaments in fibroblasts have uniform length and form super-structures, in which numerous parallel filaments are organized in registry forming filament 'stacks'. Such structures were later found in several other types of interphase non-muscle cell[8,9], as well as in the contractile ring of dividing cells[9] and circumferential actin belts of epithelial cells in the organ of Corti[10].

Recent studies using total internal reflection fluorescence (TIRF) and super-resolution microscopy, particularly structured illumination microscopy (SIM)[11,12], significantly improved the visualization of individual bipolar myosin II filaments in non-muscle cells[13–16]. Myosin II filaments were found not only in stress fibres but also in transverse arcs[15]. It was observed that they emerge at the cell periphery[15,17], sometimes in the proximity of focal adhesions[16].

This study addresses the emergence of ordered supramolecular organization of myosin II filaments in the cell and the role of their turnover and interactions with dynamic arrays of actin filaments in such organization.

SIM imaging of cells with labelled myosin II regulatory light chain (RLC) and/or myosin II heavy chain made it possible to visualize individual myosin II filaments (Fig. 1a and Supplementary Fig. 1a–c) in agreement with previous publications[7,13,15]. Myosin heads in an individual filament appeared as a 'doublet' of fluorescent spots separated by a distance of 300 ± 20 nm (Supplementary Fig. 2a–c), which corresponds to the length of myosin II filaments assembled *in vitro*[18]. It is worth noting that in REF52 cells the RLC labelling was always observed together with myosin IIA heavy chain labelling (Supplementary Fig. 1b,c), suggesting that all myosin II filaments labelled by RLC also contain myosin IIA heavy chain. We cannot exclude however that some RLC-labelled filaments contained also myosin IIB (refs 13,14) or even myosin 18 (refs 19,20). Myosin II filaments were mainly associated with actin bundles connecting focal adhesions (known as 'ventral stress fibres'[21–25]) and with transverse actin arcs in the lamellae of spreading cells[17,21,22,26] (Supplementary Fig. 1d,e).

Strikingly, myosin II filaments associated with parallel actin bundles (stress fibres or transverse arcs) were aligned into 'stacks'

[1]Mechanobiology Institute, National University of Singapore, Singapore 117411, Singapore. [2]Department of Materials and Interfaces, Weizmann Institute of Science, Rehovot 76100, Israel. [3]James Franck Institute, University of Chicago, Chicago, Illinois 60637, USA. [4]Laboratoire Matire et Systèmes Complexes, UMR 7057 CNRS & Université Paris Diderot, Paris 75013, France. [5]Advanced Imaging Center, HHMI Janelia Research Campus, Ashburn, Virginia 20147, USA. [6]Department of Molecular Cell Biology, Weizmann Institute of Science, Rehovot 76100, Israel.
[7]Correspondence should be addressed to R.Z.-B. or A.D.B. (e-mail: biezbr@nus.edu.sg or alexander.bershadsky@weizmann.ac.il)

Received 23 May 2016; accepted 15 December 2016; published online 23 January 2017; corrected after print 31 January 2017; DOI: 10.1038/ncb3466

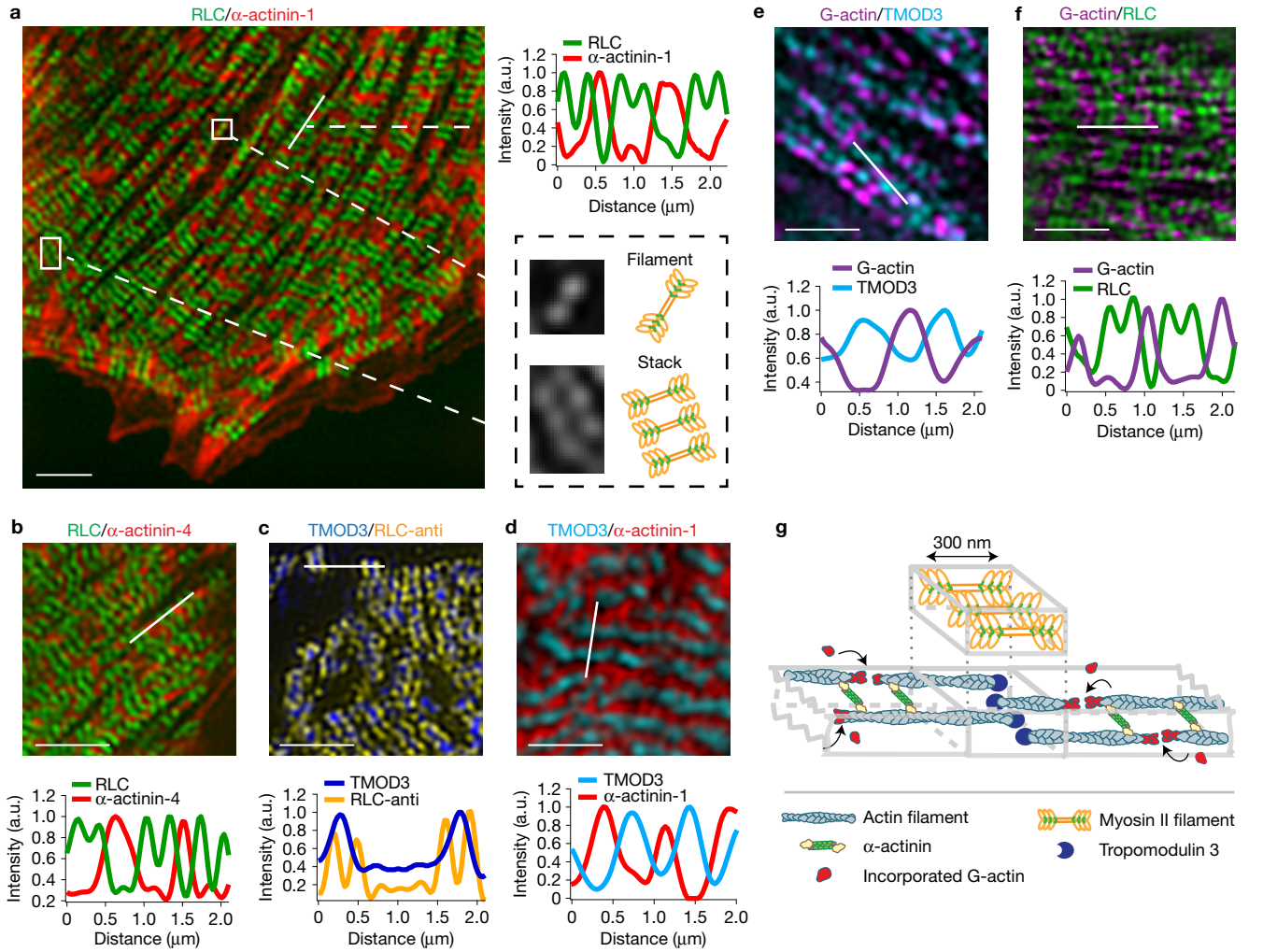

Figure 1 Localization of actin filament pointed and barbed ends relative to myosin II- and α-actinin-enriched zones of stress fibres and transverse arcs. (**a**,**b**) Complementary distribution of myosin II filaments and α-actinin-enriched domains visualized in REF52 cells co-expressing α-actinin-1-mCherry (red) and RLC-GFP (green) (**a**), or α-actinin-4-mCherry (red) and RLC-GFP (green) (**b**). For **a**, see also Supplementary Video 1. The RLC images of the boxed regions in **a** shown at high magnification in the inset on the right display an individual myosin filament and a myosin filament stack, as indicated in the schematic. The line scans of the red and green fluorescence intensities along the direction of α-actinin-1- or α-actinin-4-positive bundles (solid white lines in **a** and **b**, respectively) show complementarity between myosin filaments (double green peaks) and α-actinin-1- or -4-enriched domains (red peaks). (**c**,**d**) Pointed ends of actin filaments labelled with GFP-tropomodulin 3 (GFP-TMOD3) (shown in blue in **c** and in cyan in **d**) co-localize with myosin II filaments visualized by staining with an antibody against RLC (yellow, **c**) and alternate with α-actinin-1-enriched domains visualized by expression of α-actinin-1-mCherry (red, **d**). The graphs at the bottom of the figures represent results of the scanning of corresponding fluorescence intensities along the white lines indicated in each figure. For **d**, see also Supplementary Video 2. (**e**,**f**) Zones enriched in barbed ends of actin filaments visualized by incorporation of Alexa 568-G-actin (magenta) alternate with both pointed ends decorated by GFP-TMOD3 (cyan, **e**) and myosin II filament labelled with RLC-GFP (green, **f**). Line scans of corresponding fluorescence intensities along the direction of actin bundles (white lines) are shown at the bottom of respective figures. (**g**) Schematic depicting the organization of actin and myosin II filaments in the quasi-sarcomeric units of stress fibres or transverse arcs. A single 'sarcomere' is shown. The position of the myosin filament stack is artificially 'lifted' to provide better visualization of actin filament organization. Barbed ends of actin filaments (visualized by G-actin incorporation) are located in the α-actinin-enriched zones, while pointed ends (decorated by TMOD3) overlap with myosin filament stacks. The experiments were performed using Nikon 3D-SIM. Scale bars, 2 μm.

(Fig. 1a). These stacks did not result from overexpression of the RLC-GFP construct, since endogenous myosin II in non-transfected cells forms identical structures (Supplementary Fig. 1c). The myosin stack structures can be readily visualized in REF52 fibroblasts (Fig. 1 and Supplementary Fig. 1a–e) and also in other cell types, including HUVEC endothelial cells (Supplementary Fig. 1f). These stacks were perpendicular to the actin bundles and often spanned across 2–5 parallel neighbouring bundles (Fig. 1 and Supplementary Figs 1 and 2d–f). In agreement with numerous previous publications[22–24,27], the domains occupied by myosin filaments were separated by zones enriched in the actin crosslinking protein α-actinin (isoforms 1 and 4) (Fig. 1a,b and Supplementary Video 1).

To elucidate the topology of the arrangements of actin and myosin filaments we independently labelled the barbed (plus) and pointed (minus) ends of actin filaments defined by incorporation of labelled G-actin[28,29] and by decoration with GFP-tropomodulin 3 (refs 30,31), respectively. Such labelling revealed that the pointed ends of actin filaments were co-localized with myosin II filaments (Fig. 1c) and

alternated with the α-actinin-rich zones (Fig. 1d and Supplementary Video 2). The barbed ends alternated with the zones containing pointed ends (Fig. 1e) and myosin filaments (Fig. 1f). Taken together, these observations confirm and extend the quasi-sarcomeric model of organization of actomyosin bundles in non-muscle cells (Fig. 1g and refs 10,23,25). However, unlike muscle myofibrils, sarcomeric non-muscle actin bundles demonstrated pronounced variability in the length of α-actinin-enriched domains (Supplementary Fig. 2g–i).

The myosin II filament stacks participated in global processes of actin flow in the cell. Such flow was observed both at the stress fibres and centripetal arcs, although the motions of myosin II filaments at these two locations were different. The stacks of myosin filaments associated with transverse arcs moved centripetally together with these arcs (Supplementary Fig. 3a and Supplementary Videos 3 and 4) with the velocity increasing during the translocation from the cell edge toward the centre and approaching the maximal level of 0.15 μm min^{-1} at a distance of 10–15 μm from the cell edge (Supplementary Fig. 3c). At the central part of the cell, the arcs bearing the myosin stacks underwent rapid contraction and disassembled (Supplementary Video 3).

The movement of the myosin stacks associated with parallel, ventral stress fibres was on average slower than the centripetal movement of transverse arcs. The zones of maximal centripetal velocity (0.07–0.08 μm min^{-1}) were at the periphery of the cell (Supplementary Fig. 3d). The centripetal movement slowed down closer to the cell centre, approaching zero at 15–20 μm from the edge, and then changed direction to centrifugal (Supplementary Fig. 3b,d). The positions corresponding to the reversal of the direction of myosin movement were correlated between neighbouring stress fibres, demarcating two zones characterized by opposite directions of myosin movement. In general, the myosin stacks bridging two or more parallel stress fibres moved as single entities (Supplementary Videos 5 and 6).

To investigate the turnover of myosin molecules forming the myosin filaments and stacks, we used fluorescence recovery after photobleaching (FRAP). In these experiments, we expressed the markers of myosin heads, RLC-GFP or MHC-IIA-GFP, together with actin-mCherry, and photobleached both in a small circular area (2 μm diameter) containing myosin stacks. We found that myosin stacks, as well as doublet fluorescent spots corresponding to individual myosin filaments, gradually recovered their fluorescence (with a half-time of about one minute) reaching a plateau value that was lower than the initial fluorescence level, thereby indicating a non-zero, immobile fraction (Fig. 2a,b andSupplementary Videos 7 and 8). Since an individual filament consists of about 30 myosin II molecules[18], the gradual recovery of myosin II filament fluorescence is not surprising. The non-zero immobile fraction suggests that the filaments may have a 'core' consisting of several myosin II molecules, which turnover much slower than the ones located near the filament surface. FRAP kinetics of RLC (Supplementary Video 7) and MHC-IIA (Supplementary Video 8) were similar (Fig. 2a,b,d). These data suggest that during turnover, myosin light and heavy chains are incorporated into filaments together and disassociation of the light chain from the heavy chain is negligible.

The observations of actin FRAP in the same location showed a recovery rate comparable to that of myosin (Fig. 2c,d). To check whether the turnover kinetics of myosin filaments depends on the dynamics of the actin filaments with which they interact, we suppressed actin dynamics by combined treatment with inhibitors of actin polymerization and depolymerization, as described previously[32]. We found that even when actin filament turnover was substantially inhibited (with immobile fraction around 80%) (Fig. 2f,g), myosin filaments still turned over with rates similar to those in control cells (Fig. 2e,g,h and Supplementary Video 9). Thus, turnover of myosin molecules in the filaments comprising the stacks does not depend on actin filament dynamics.

The next stage of myosin self-organization, association of myosin filaments into stacks, proceeded through a series of assembly events (Fig. 3 and Supplementary Videos 10–14). When it was possible to resolve, we observed that even single myosin filaments moved in association with actin fibres (Fig. 3a,b and Supplementary Videos 10–12). Typical 'elementary' assembly processes included 'in registry' alignment of two myosin filaments moving along parallel tracks (Fig. 3a and Supplementary Video 10), or movement of myosin filaments associated with different actin bundles towards each other along with parallel alignment of these bundles and shortening the distance between them (Fig. 3b and Supplementary Videos 11 and 12). Two stacks adjacent to each other could further align and fuse forming a longer stack (Fig. 3c and Supplementary Video 13).

The example in Fig. 3d (Supplementary Video 14) shows a more complex process of incorporation of individual myosin filaments into a stack. The filament (indicated by yellow arrows) travelled for a substantial (micrometre) distance before approaching another filament (arrowhead) associated with a prominent actin bundle. During this translocation (frames 8–12 min), the first filament underwent apparent splitting into two via the formation of an intermediate '3-motor-group' (asterisk) as previously described[9]. After splitting, the 'daughter' filaments detached from each other and one of them (white arrow) attached to the pre-existing filament (arrowhead).

Thus, processes of stack formation from individual filaments proceed with a characteristic time of minutes and involve long-range movements of the filaments towards each other with occasional filament splitting events. Myosin filament movements leading to their registered organization occurred in association with the actin fibres and were accompanied by alignment of these fibres into parallel arrays.

To reveal the factors involved in myosin stack formation, we studied the process of actomyosin network recovery after its disruption by the Rho kinase inhibitor Y27632. Treatment of the cells with Y27632 led to complete disassembly of the myosin filaments that appeared again after inhibitor washout and formed prominent stacks (Fig. 4a and Supplementary Video 15). Actin bundles partially disappeared following Y27632 treatment but fully recovered after inhibitor washout (Fig. 4a and Supplementary Videos 16 and 17).

Analysis of the process of stack recovery after Y27632 washout in the presence of blebbistatin, an inhibitor of myosin ATPase, revealed that *de novo* formation of individual myosin filaments was only slightly (if at all) reduced by blebbistatin, while myosin stack formation was essentially blocked (Fig. 4b). Concomitant addition of inhibitors of actin polymerization and depolymerization, latrunculin A and jasplakinolide (Fig. 4c), as well as inhibition of formin-dependent actin polymerization by SMIFH2 (Fig. 4d), also prevented formation of myosin stacks during recovery from Y27632; removal of SMIFH2 permitted full recovery of the stacks (Fig. 4d).

Consistently, the treatment of control cells with either the myosin II inhibitor blebbistatin (Supplementary Fig. 5a), or actin dynamics

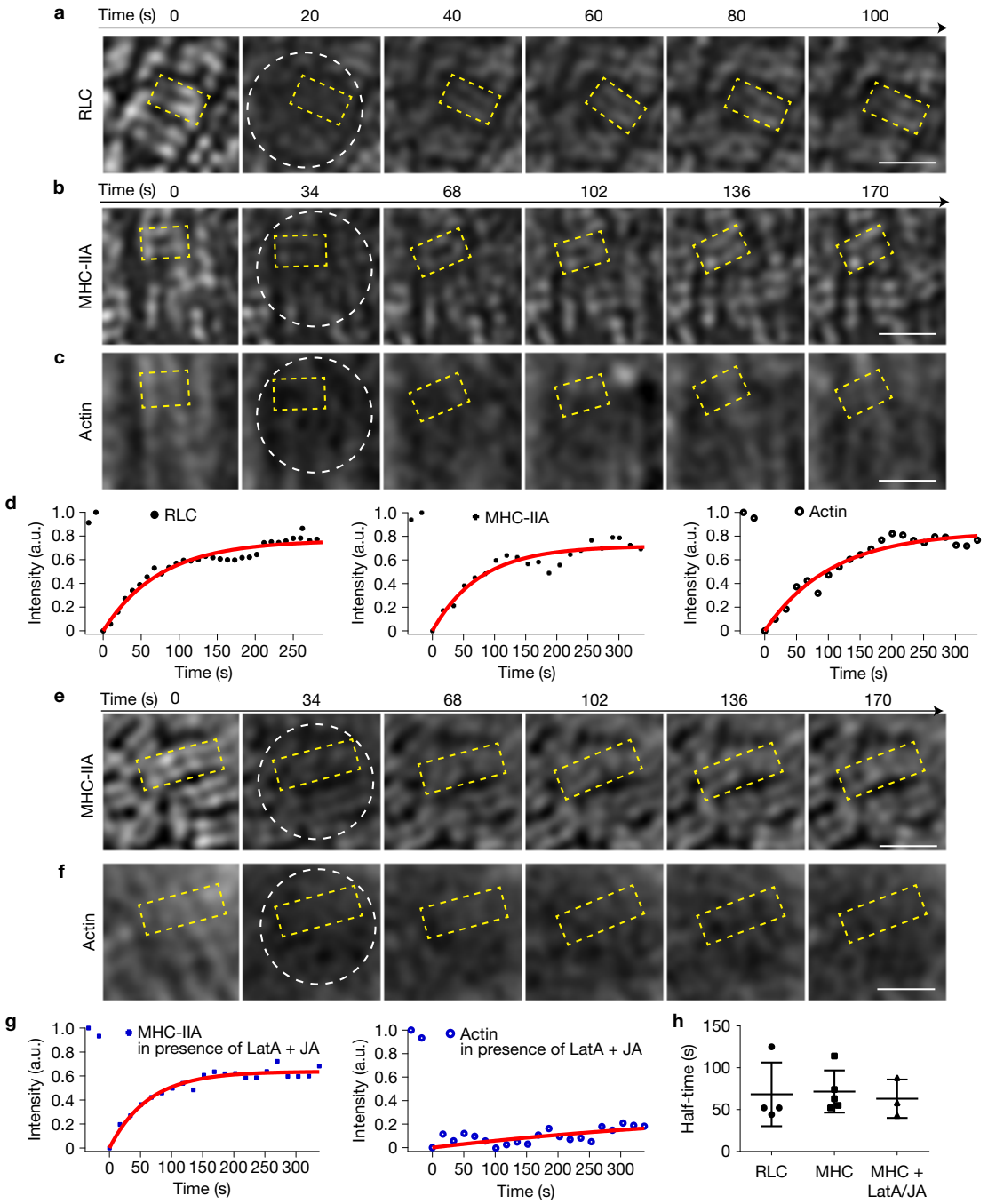

Figure 2 Turnover of individual myosin II filaments revealed by fluorescence recovery after photobleaching (FRAP). (**a**,**b**) FRAP of the myosin filaments was observed using SIM imaging of cells expressing either RLC-GFP (**a**) or MHC-IIA-GFP (**b**). (**c**) FRAP images of actin-mCherry in the same field as in **b**. See also Supplementary Videos 7 and 8. The bleached region was a circle (2 μm diameter, white circumference); the bleached myosin stack followed during the recovery is indicated by a yellow box. (**d**) Typical FRAP measurements. The details of the measurement are shown in Supplementary Fig. 4. The measurements for both RLC ($n=4$ cells) and MHC-IIA ($n=5$ cells) demonstrated similar quick recovery with dissociation rates K_{off} of 0.012 ± 0.004 and $0.010\pm0.003\,s^{-1}$ respectively, half-times of 68 ± 38 and 72 ± 25 s, respectively, and immobile fractions of $27\pm4\%$ and $25\pm12\%$, respectively. Actin FRAP in the same location as MHC-IIA showed a slightly slower recovery rate (with K_{off} $0.010\,s^{-1}$, half-time 73 s and immobile fraction 16%, see the right panel of **d**). (**e**–**g**) To observe myosin filament recovery in cells with suppressed actin filament dynamics, we treated cells expressing MHC-IIA-GFP (**e**) and actin-mCherry (**f**) with a combination of 100 nM latrunculin A (LatA) and 1 μM jasplakinolide (JA) (Supplementary Video 9). Such treatment increased the immobile fraction of actin to about 80% (**f**,**g**). The dynamics of MHC-IIA in cells treated with latrunculin A and jasplakinolide was characterized by K_{off} $0.012\pm0.004\,s^{-1}$, half-time 63 ± 23 s and immobile fraction $30\pm7\%$ ($n=3$). (**h**) The difference between recovery half-time for RLC ($n=4$ cells) and MHC-IIA ($n=5$ cells) was non-significant ($P=0.88$ by two-tailed unpaired Student's t-test), and the difference between recovery half-time for MHC-IIA in non-treated cells ($n=5$ between recovery half-time for MHC-IIA in non-treated cells ($n=5$ cells) and in cells treated with latrunculin A and jasplakinolide ($n=3$ cells) was also non-significant ($P=0.65$ by two-tailed unpaired Student's t-test). The results of the measurements above are all presented in the form of mean ± s.d. and error bars represent standard deviation (s.d.) values. The FRAP experiments were performed using Nikon 3D-SIM. Scale bars, 1 μm.

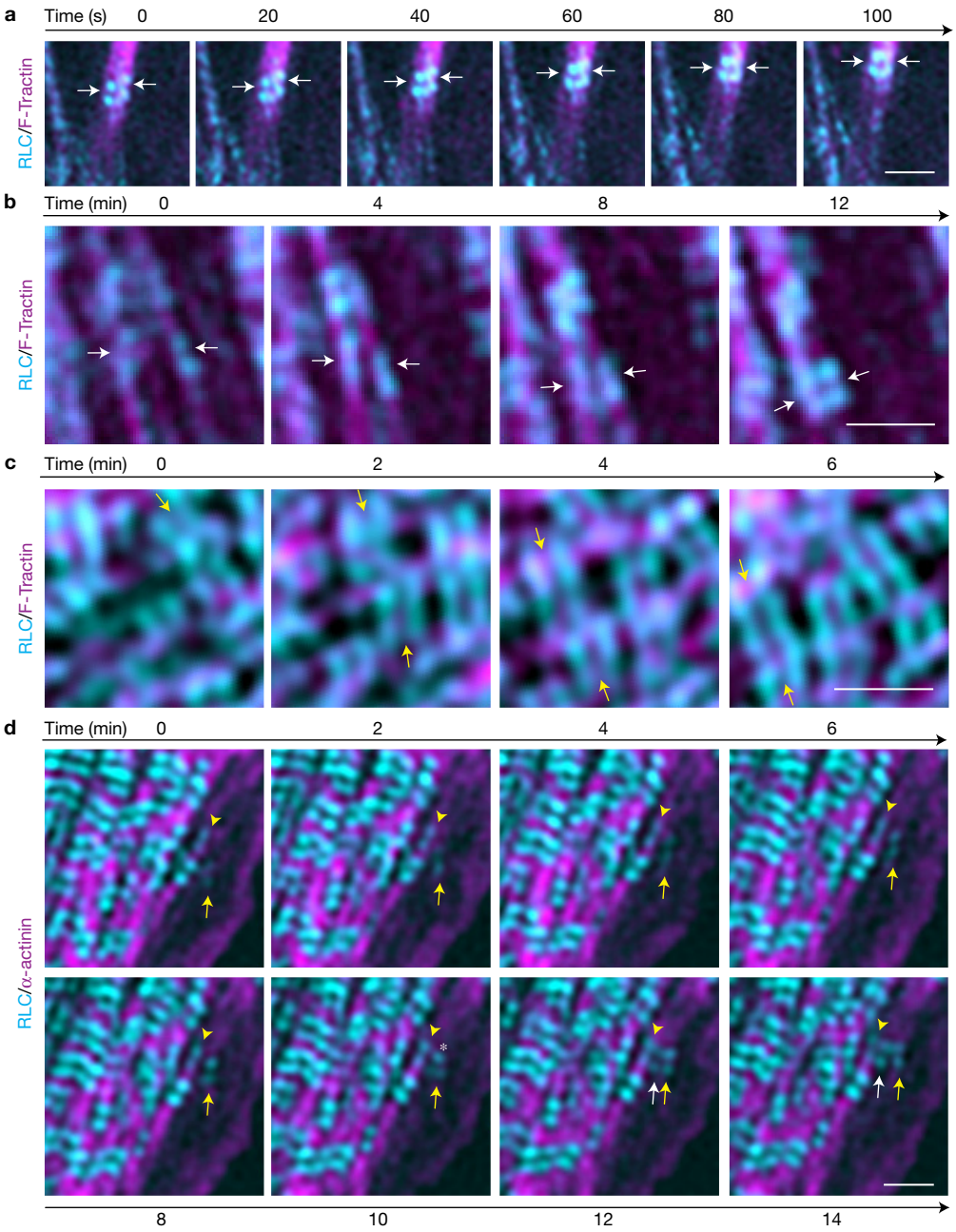

Figure 3 Establishment of registered organizations of myosin II filaments in the course of filament movements. REF52 cells expressing RLC-GFP (shown in cyan) together with F-Tractin-tdTomato (**a**–**c**) or α-actinin-mCherry (**d**) (both shown in magenta) were used for the observations. (**a**) Two parallel but shifted relative to each other myosin II filaments (arrows) associated with an actin bundle move towards each other along the actin bundle and eventually form a stable stack (see also Supplementary Video 10). Both longitudinal and perpendicular distance between the filaments decreased. (**b**) Formation of a stack between two myosin filaments (arrows) associated with separate actin fibres via movement of the filaments along the fibres and a diminishing of the distance between these fibres, so that formation of the myosin filament stacks was accompanied by formation of parallel packed actin bundles (see also Supplementary Video 11). (**c**) The alignment of two myosin filament stacks (yellow arrows) into one single stack. The merged longer stack bridges three actin bundles (see also Supplementary Video 13). (**d**) The individual myosin filament indicated by the yellow arrow moved a distance of about one micrometre towards another filament (indicated by the yellow arrowhead) (see also Supplementary Video 14). When the two filaments were close to each other (the frames corresponding to 8–10 min) the first filament underwent 'splitting' into two via the formation of the characteristic '3-motor-group' (asterisk) described in ref. 9. After splitting, the 'daughter' filaments separated from each other and one of them (white arrow) attached to the pre-existing filament (yellow arrowhead). Images in **a** were captured with TIRF-SIM, and images in **b**–**d** with Nikon 3D-SIM. Scale bars, 1 μm.

inhibitors latrunculin A/jasplakinolide (Supplementary Fig. 5b), or formin inhibitor SMIFH2 (Supplementary Fig. 5c) led to prominent deterioration of the myosin stacks.

We further performed a small interfering RNA (siRNA) screen to reveal the actin-associated proteins involved in the myosin II registered organization. Altogether, we checked 28 actin-associated proteins,

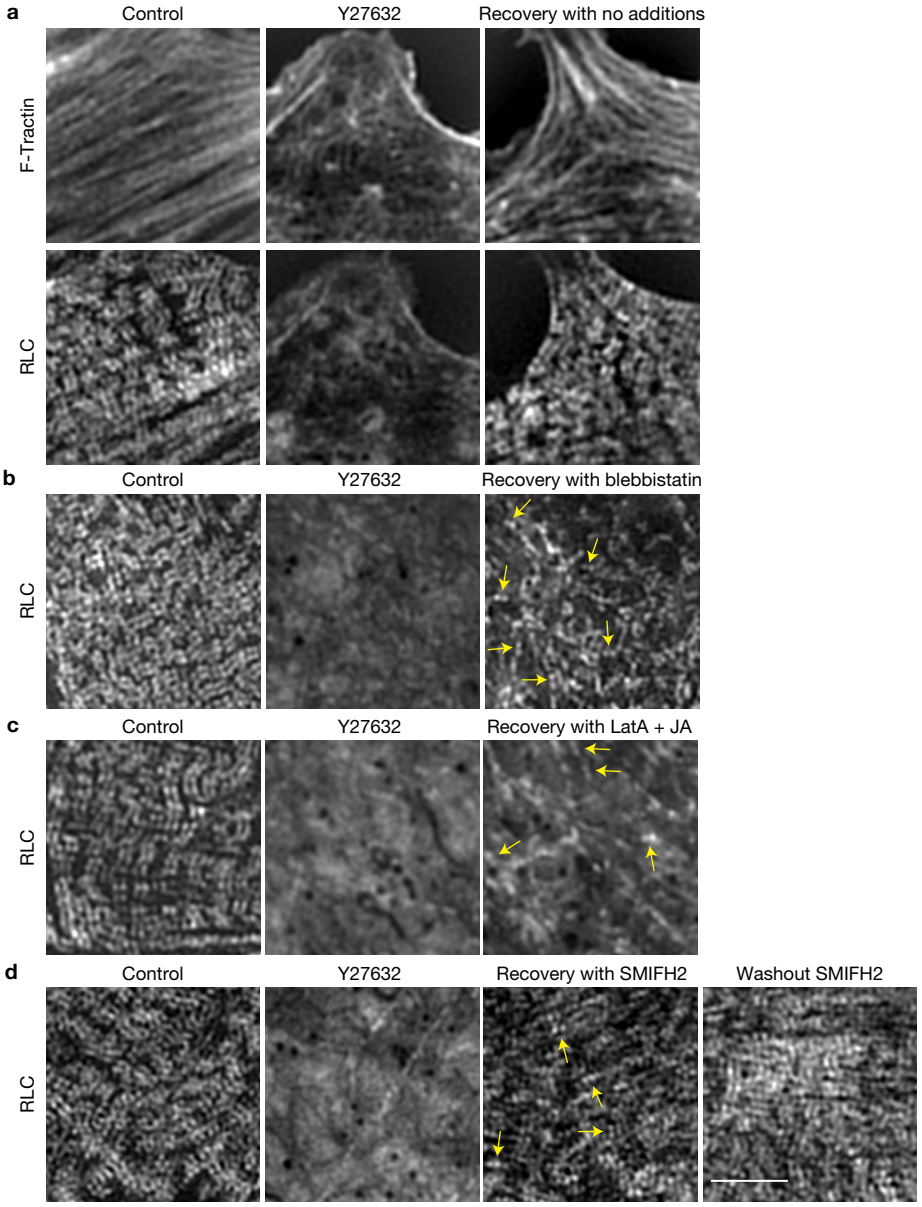

Figure 4 Recovery of myosin II stacks depends on both myosin II ATPase activity and actin filament dynamics. (**a**) Actin filaments (F-Tractin-tdTomato, upper row) and myosin light chain (RLC-GFP, second row from top) are labelled. The figure shows the evolution of actin and myosin organization in the same field. Middle images show that treatment of cells with the Rho kinase inhibitor Y27632 (20 μM) for 25 min led to complete disassembly of myosin filaments and disorganization of the system of actin bundles. The disassembly is fully reversible and the myosin II stacks completely recovered 15 min following drug washout along with reformation of the actin filament bundles (right images). (**b**) The myosin pattern shown in the left image was completely disrupted by treatment with Y27632 (middle image), and recovered for 15 min following Y27632 washout in the presence of blebbistatin (40 μM, right image). Note that individual myosin filaments recovered (arrows in the right image), but formation of myosin filament stacks was suppressed. (**c**) The myosin pattern shown in the same field before treatment (left column), after 25 min incubation in 20 μM Y27632 (middle column), and following 15 min of recovery from Y27632 in the presence of a combination of 100 nM latrunculin A (LatA) and 1 μM jasplakinolide (JA) (right column). Individual myosin filaments (arrows) recover under these conditions, while formation of myosin filament stacks is completely suppressed. (**d**) The myosin pattern shown in the left image was completely disrupted by treatment with Y27632 (second image from left), and recovered for 20 min following Y27632 washout in the presence of SMIFH2 (15 μM, third image from left). Then the SMIFH2 was washed out and the cell recovered for an additional 40 min (right image). Note that SMIFH2 did not interfere with recovery of individual myosin filaments (arrows), but prevented the formation of myosin stacks, which recovered only after washout of SMIFH2. The experiments were performed using Nikon 3D-SIM. The scale bar, 3 μm, is the same for all images.

including proteins regulating actin assembly, disassembly and crosslinking. Full results of this analysis will be published elsewhere; here we present only the data concerning proteins whose knockdown significantly disrupted the formation of the myosin II filament stacks.

REF52 cells express two α-actinin isoforms, α-actinin-1 and α-actinin-4, both of which alternate with myosin II filament domains along stress fibres and transverse arcs (Fig. 1a,b). Knockdown of α-actinin-4 resulted in severe changes in the organization of stress

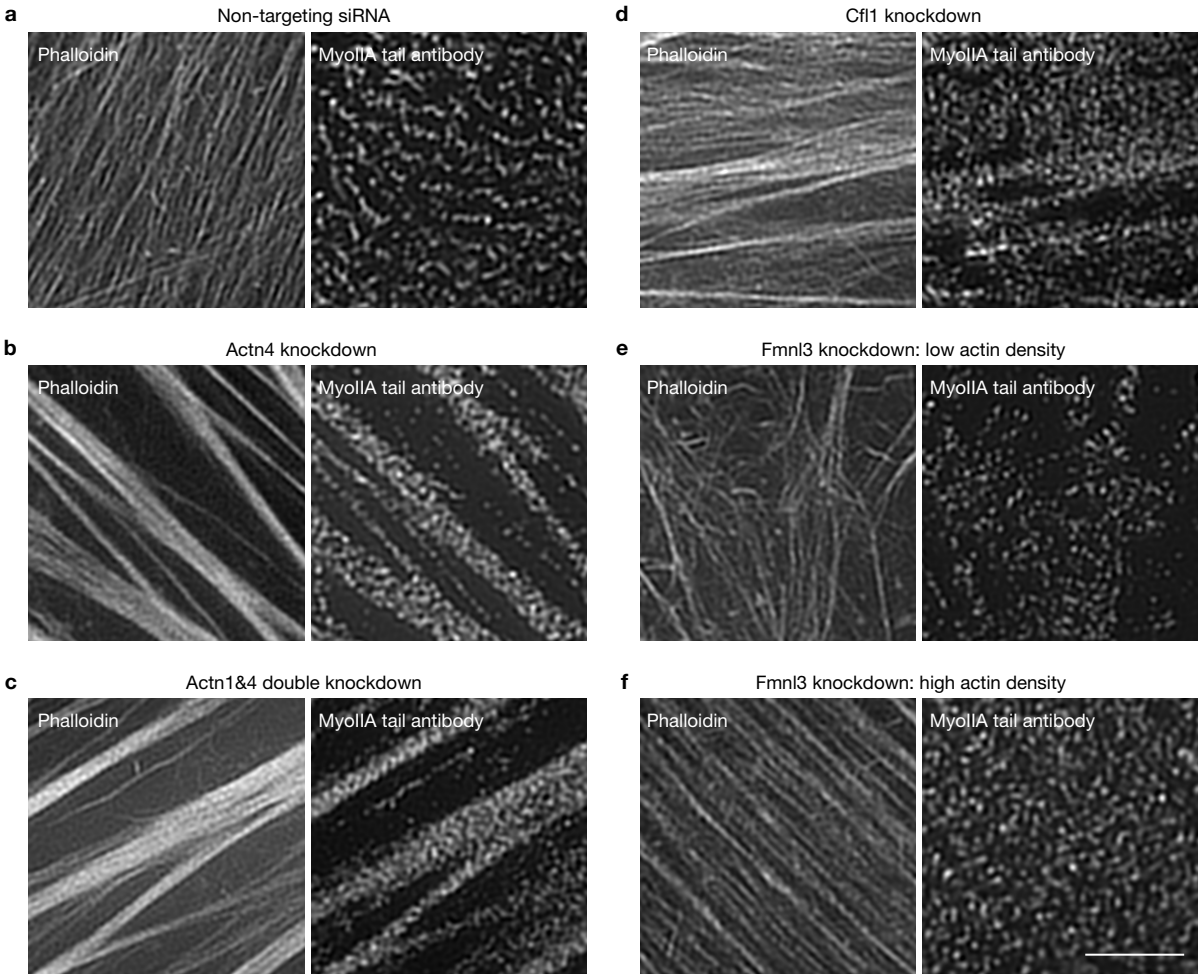

Figure 5 Registered organization of myosin IIA filaments depends on actin-associated proteins. (**a**) Control cells (transfected with a non-targeting siRNA pool) displayed parallel actin stress fibres visualized by staining with phalloidin Alexa-Fluor 488 (left) and typical myosin II filament stacks visualized by immunofluorescence with antibody against myosin IIA heavy chain tail domain perpendicular to the actin fibres (right). (**b**,**c**) Knockdown of α-actinin-4 (Actn4) or double knockdown of α-actinin-1 and -4 (Actn1&4) resulted in reduction of the number and increase of thickness of the actin stress fibres (left). The registered organization of myosin IIA filaments was completely disrupted (right). (**d**) Knockdown of cofilin1 (Cfl1) resulted in denser organization of the actin fibres (left) and disruption of myosin II stacks (right). (**e**,**f**) Formin Fmnl3 knockdown led to a pronounced decrease in the average actin filament density (**e**, left) and disruption of myosin II filament registered organization (**e**, right); note that the disruption of myosin II filament organization was observed even in cells still preserving relatively high actin filament density (**f**). The images were captured with Nikon 3D-SIM. The scale bar, 3 μm, is the same for all images.

fibres: instead of numerous parallel actin fibres associated with myosin II stacks (Fig. 5a), the cell formed wider-spaced thicker bundles with disordered organization of myosin IIA filaments (Fig. 5b). Thus, α-actinin-4 is critically important for the myosin filament stack formation in REF52 cells. The knockdown of α-actinin-1 disrupted myosin II organization to a lesser degree than the knockdown of α-actinin-4, and the double knockdown of α-actinin-1 and -4 produced a phenotype similar to that produced by knockdown of α-actinin-4 alone (Fig. 5c). The knockdown of several other actin filament crosslinking proteins (filamin-A, plastin3, fascin, supervillin) did not result in a prominent phenotype.

Another protein that appeared to be indispensable for the registered organization of myosin filaments was cofilin1, a known actin filament severing and depolymerizing factor[33] that may compete with myosin II for binding to actin filaments[34]. The knockdown of cofilin1 resulted in denser organization of actin fibres and myosin filaments with completely disrupted myosin II stacks (Fig. 5d). This result, along with our data on inhibition of myosin II stack organization by treatment with latrunculin A/jasplakinolide, strongly suggests that actin turnover is necessary for the formation and maintenance of myosin II filament stacks.

Finally, we identified a particular formin required for myosin stack formation in REF52 cells. Knockdown of formin-like protein 3 (Fmnl3) but not several other formins (Diaph1, Diaph2, Diaph3, Daam1, Daam2, Fmnl1, Fhod1) reduced the average density of actin fibres and disrupted the registered organization of myosin II filaments (Fig. 5e). The effect of Fmnl3 knockdown on myosin organization did not depend on the reduction of actin density since it was apparent also in cells where the density of actin network was still high (Fig. 5f).

In this study, we followed the processes of supramolecular organization of myosin II filaments in the course of their interactions

with arrays of actin filaments using SIM and fluorescence labelling of myosin II filaments. A significant feature of myosin II filaments in non-muscle cells is their fast turnover with a half-time of FRAP of about one minute, while in skeletal muscle cells it takes more than an hour[35]. The assembly of myosin filaments into stacks represents a higher level of organization compared with individual filament turnover. The characteristic time for the registered organization of myosin filaments is significantly longer than the characteristic filament turnover time. The process of stack organization requires myosin II motor activity, involves long-range (micrometre scale) myosin filament movements and, unlike individual myosin II filament turnover, strongly depends on the dynamics of associated actin filaments. siRNA knockdown revealed a function for the actin depolymerizing protein cofilin1, actin polymerizing protein formin Fmnl3, and actin filament crosslinking protein α-actinin-4 in establishment of myosin IIA filament registered organization.

Possible molecular processes leading to the formation of myosin II filament stacks require special consideration. Two recent studies[9,36] show that new myosin II filaments can emerge in proximity to each other, in a sequence of events termed 'expansion'. The expansion could be a result of filament splitting[9] or 'templated nucleation' when pre-existing filaments serve as templates facilitating assembly of novel filaments[36]. These models suggest that the stacks could form as a result of sequential expansion events. The discovery of filament expansion opens a new facet in the process of myosin II filament assembly. Of note, the sequential amplification of myosin II filaments was shown to be an actin filament-dependent process[36] consistent with our findings that the formation of myosin II filament stacks depends on both myosin II mechanochemical activity and actin assembly/disassembly. Further studies are required to elucidate whether actin regulators such as cofilin1, Fmnl3 and α-actinin-4 affect the myosin stack organization by changing the probability of myosin filament expansion.

While we confirmed occasional myosin filament duplication in our experiments, the newly formed daughter filaments often moved apart from each other rather than remaining associated (see Fig. 3d). In our view, the existence of attractive forces between individual filaments is required to explain why stacks originally formed by filament 'expansion' would maintain their integrity against a variety of disordering forces present in the cytoskeleton—random molecular-scale and motor-driven noise as well as fluctuations of the actin through assembly/disassembly processes.

Our observations suggest the existence of long-range interactions between the myosin filaments in separated bundles. Long-range movements of individual filaments and filament stacks during their alignment into registry (Fig. 3), as well as preservation of the registered organization of parallel myosin filaments separated by more than 100 nm gaps (Fig. 1a), imply that individual myosin filaments may 'sense' and 'attract' each other through the surrounding medium.

The mechanism we propose involves the transmission of contractile forces via the intervening, initially disordered, actin network (see Supplementary Videos 16 and 17) between two myosin filaments that are not in direct contact, for example, between a filament associated with one actin bundle and its neighbour associated with another bundle. In addition to the registry, this mechanism can also explain a decrease in the transverse distance between neighbouring actin fibres (such as seen in Fig. 3b) since elastic interactions also result in attractive forces in the direction transverse to the myosin filament orientation[37]. Mechanical (elastic) interactions that transmit forces emerging due to actomyosin contractility were quantitatively analysed to explain self-organization in simple actomyosin networks *in vitro*[38] as well as large-scale cytoskeletal and sarcomeric organization in stress fibres[39] and muscle cells[37], respectively.

While registry is the 'mechanical equilibrium' configuration, towards which interacting myosin filaments evolve[37,40], the actual dynamics that governs how two myosin filaments align in a registered manner is complex and requires a detailed, dynamical picture of the stress fibres and the intervening disordered actin network to model. In particular, since the myosin filaments tend to be localized at the pointed ends of the actin filaments and, therefore, can hardly move freely along the actin bundles composed of actin filaments with alternating polarity, continuous actin remodelling due to assembly/disassembly is essential for the process of registry. These complex rearrangements take time and are consistent with the observation that the process of registry is significantly slower than myosin filament turnover.

Since the interaction of myosin filaments associated with different actin bundles creates forces attracting these bundles towards each other, the organization of myosin filaments into stacks is a plausible mechanism for the formation of the densely packed arrays of parallel actin bundles often observed in polarized fibroblast-type cells. Thus, we hypothesize that the myosin stacks may serve as cytoskeletal elements coordinating mutual positions and movements of the neighbouring actin bundles (stress fibres or arcs). Finally, registered organization of the myosin filaments could also regulate cellular contractility[41], which could be important in the processes of focal adhesion formation, matrix remodelling and fibrillogenesis. All in all, interaction between myosin II filaments leading to their registered organization is an important element in the process of actin cytoskeleton self-organization determining the architecture of the cell. □

METHODS

Methods, including statements of data availability and any associated accession codes and references, are available in the online version of this paper.

Note: Supplementary Information is available in the online version of the paper

ACKNOWLEDGEMENTS

We thank J. R. Sellers and V. Viasnoff for helpful discussions, MBI microscopy core facility for technical support, and H.-T. Ong for help with PIV analysis of movements of myosin filaments. We thank the Advanced Imaging Center, Janelia Research Campus for the support using high-temporal-resolution TIRF-SIM, in particular, the help from L. Shao and S. Khuon. The Advanced Imaging Center is generously supported by the Gordon and Betty Foundation as well as the Howard Hughes Medical Institute. This research has been supported by the National Research Foundation Singapore, Ministry of Education of Singapore, Grant R-714-006-006-271 (awarded to A.D.B.), Ministry of Education Tier2 grant MOE2015-T2-1-045 (awarded to R.Z.-B.), and administrated by the National University of Singapore. S.A.S. is grateful to the Israel Science Foundation and the Schmidt Minerva Center, and the US-Israel Binational Science Foundation for their support as well as a research grant from Mr and Mrs Antonio Villalon. A.D.B. also holds the Joseph Moss Professorial Chair in Biomedical Research at the Weizmann Institute of Science, Israel.

AUTHOR CONTRIBUTIONS

A.D.B. conceived the study. S.H., Z.G., P.H., R.Z.-B. and A.D.B. designed the research. S.H. performed the research; V.T. and Y.-H.T. contributed to

immunofluorescence experiments; T.-L.C. contributed to TIRF-SIM experiments; K.D. and S.A.S. discussed the results and suggested a hypothesis based on the physical model. S.H., R.Z.-B. and A.D.B. analysed data and wrote the manuscript with input from all authors.

COMPETING FINANCIAL INTERESTS

The authors declare no competing financial interests.

Published online at http://dx.doi.org/10.1038/ncb3466
Reprints and permissions information is available online at www.nature.com/reprints

1. Langanger, G. *et al.* The molecular organization of myosin in stress fibers of cultured cells. *J. Cell Biol.* **102,** 200–209 (1986).
2. Verkhovsky, A. B., Svitkina, T. M. & Borisy, G. G. Myosin II filament assemblies in the active lamella of fibroblasts: their morphogenesis and role in the formation of actin filament bundles. *J. Cell Biol.* **131,** 989–1002 (1995).
3. Lazarides, E. & Weber, K. Actin antibody: the specific visualization of actin filaments in non-muscle cells. *Proc. Natl Acad. Sci. USA* **71,** 2268–2272 (1974).
4. Weber, K. & Groeschel-Stewart, U. Antibody to myosin: the specific visualization of myosin-containing filaments in nonmuscle cells. *Proc. Natl Acad. Sci. USA* **71,** 4561–4564 (1974).
5. Lazarides, E. & Burridge, K. Alpha-actinin: immunofluorescent localization of a muscle structural protein in nonmuscle cells. *Cell* **6,** 289–298 (1975).
6. Gordon, W. E. III Immunofluorescent and ultrastructural studies of "sarcomeric" units in stress fibers of cultured non-muscle cells. *Exp. Cell Res.* **117,** 253–260 (1978).
7. Svitkina, T. M., Verkhovsky, A. B., McQuade, K. M. & Borisy, G. G. Analysis of the actin-myosin II system in fish epidermal keratocytes: mechanism of cell body translocation. *J. Cell Biol.* **139,** 397–415 (1997).
8. Goeckeler, Z. M., Bridgman, P. C. & Wysolmerski, R. B. Nonmuscle myosin II is responsible for maintaining endothelial cell basal tone and stress fiber integrity. *Am. J. Physiol. Cell Physiol.* **295,** C994–1006 (2008).
9. Fenix, A. M. *et al.* Expansion and concatenation of non-muscle myosin IIA filaments drive cellular contractile system formation during interphase and mitosis. *Mol. Biol. Cell* **27,** 1465–1478 (2016).
10. Ebrahim, S. *et al. Curr. Biol.* **23,** 731–736 (2013).
11. Gustafsson, M. G. Surpassing the lateral resolution limit by a factor of two using structured illumination microscopy. *J. Microsc.* **198,** 82–87 (2000).
12. Kner, P., Chhun, B. B., Griffis, E. R., Winoto, L. & Gustafsson, M. G. Super-resolution video microscopy of live cells by structured illumination. *Nat. Methods* **6,** 339–342 (2009).
13. Beach, J. R. *et al.* Nonmuscle myosin II isoforms coassemble in living cells. *Curr. Biol.* **24,** 1160–1166 (2014).
14. Shutova, M. S., Spessott, W. A., Giraudo, C. G. & Svitkina, T. Endogenous species of mammalian nonmuscle myosin IIA and IIB include activated monomers and heteropolymers. *Curr. Biol.* **24,** 1958–1968 (2014).
15. Burnette, D. T. *et al.* A contractile and counterbalancing adhesion system controls the 3D shape of crawling cells. *J. Cell Biol.* **205,** 83–96 (2014).
16. Pasapera, A. M. *et al.* Rac1-dependent phosphorylation and focal adhesion recruitment of myosin IIA regulates migration and mechanosensing. *Curr. Biol.* **25,** 175–186 (2015).
17. Burnette, D. T. *et al.* A role for actin arcs in the leading-edge advance of migrating cells. *Nat. Cell Biol.* **13,** 371–381 (2011).
18. Billington, N., Wang, A., Mao, J., Adelstein, R. S. & Sellers, J. R. Characterization of three full-length human nonmuscle myosin II paralogs. *J. Biol. Chem.* **288,** 33398–33410 (2013).
19. Billington, N. *et al.* Myosin 18A coassembles with nonmuscle myosin 2 to form mixed bipolar filaments. *Curr. Biol.* **25,** 942–948 (2015).
20. Heissler, S. M. & Sellers, J. R. Four things to know about myosin light chains as reporters for non-muscle myosin-2 dynamics in live cells. *Cytoskeleton* **72,** 65–70 (2015).
21. Small, J. V., Rottner, K., Kaverina, I. & Anderson, K. I. Assembling an actin cytoskeleton for cell attachment and movement. *Biochim. Biophys. Acta* **1404,** 271–281 (1998).
22. Hotulainen, P. & Lappalainen, P. Stress fibers are generated by two distinct actin assembly mechanisms in motile cells. *J. Cell Biol.* **173,** 383–394 (2006).
23. Burridge, K. & Wittchen, E. S. The tension mounts: stress fibers as force-generating mechanotransducers. *J. Cell Biol.* **200,** 9–19 (2013).
24. Kassianidou, E. & Kumar, S. A biomechanical perspective on stress fiber structure and function. *Biochim. Biophys. Acta* **1853,** 3065–3074 (2015).
25. Tojkander, S., Gateva, G. & Lappalainen, P. Actin stress fibers–assembly, dynamics and biological roles. *J. Cell Sci.* **125,** 1855–1864 (2012).
26. Heath, J. P. Direct evidence for microfilament-mediated capping of surface receptors on crawling fibroblasts. *Nature* **302,** 532–534 (1983).
27. Peterson, L. J. Simultaneous stretching and contraction of stress fibers *in vivo*. *Mol. Biol. Cell* **15,** 3497–3508 (2004).
28. Shestakova, E. A., Singer, R. H. & Condeelis, J. The physiological significance of β-actin mRNA localization in determining cell polarity and directional motility. *Proc. Natl Acad. Sci. USA* **98,** 7045–7050 (2001).
29. Symons, M. H. & Mitchison, T. J. Control of actin polymerization in live and permeabilized fibroblasts. *J. Cell Biol.* **114,** 503–513 (1991).
30. Yamashiro, S., Gokhin, D. S., Kimura, S., Nowak, R. B. & Fowler, V. M. Tropomodulins: pointed-end capping proteins that regulate actin filament architecture in diverse cell types. *Cytoskeleton* **69,** 337–370 (2012).
31. Yamashiro, S. *et al.* Differential actin-regulatory activities of Tropomodulin1 and Tropomodulin3 with diverse tropomyosin and actin isoforms. *J. Biol. Chem.* **289,** 11616–11629 (2014).
32. Peng, G. E., Wilson, S. R. & Weiner, O. D. A pharmacological cocktail for arresting actin dynamics in living cells. *Mol. Biol. Cell* **22,** 3986–3994 (2011).
33. Bernstein, B. W. & Bamburg, J. R. ADF/cofilin: a functional node in cell biology. *Trends Cell Biol.* **20,** 187–195 (2010).
34. Wiggan, O., Shaw, A. E., DeLuca, J. G. & Bamburg, J. R. ADF/cofilin regulates actomyosin assembly through competitive inhibition of myosin II binding to F-actin. *Dev. Cell* **22,** 530–543 (2012).
35. Ojima, K., Ichimura, E., Yasukawa, Y., Wakamatsu, J. & Nishimura, T. Dynamics of myosin replacement in skeletal muscle cells. *Am. J. Physiol. Cell Physiol.* **309,** C669–C679 (2015).
36. Beach, J. R. *et al.* Actin dynamics and competition for myosin monomer govern the sequential amplification of myosin filaments. *Nat. Cell Biol.* http://dx.doi.org/10.1038/ncb3463 (2017).
37. Dasbiswas, K., Majkut, S., Discher, D. E. & Safran, S. A. Substrate stiffness-modulated registry phase correlations in cardiomyocytes map structural order to coherent beating. *Nat. Commun.* **6,** 6085 (2015).
38. Soares e Silva, M. *et al.* Active multistage coarsening of actin networks driven by myosin motors. *Proc. Natl Acad. Sci. USA* **108,** 9408–9413 (2011).
39. Zemel, A., Rehfeldt, F., Brown, A. E. X., Discher, D. E. & Safran, S. A. Optimal matrix rigidity for stress-fibre polarization in stem cells. *Nat. Phys.* **6,** 468–473 (2010).
40. Friedrich, B. M., Buxboim, A., Discher, D. E. & Safran, S. A. Striated acto-myosin fibers can reorganize and register in response to elastic interactions with the matrix. *Biophys. J.* **100,** 2706–2715 (2011).
41. Majkut, S. *et al.* Heart-specific stiffening in early embryos parallels matrix and myosin expression to optimize beating. *Curr. Biol.* **23,** 2434–2439 (2013).

DOI: 10.1038/ncb3466

METHODS

Cell culture and transfection. No cell lines used in this study were found in the database of commonly misidentified cell lines that is maintained by ICLAC and NCBI Biosample. The rat embryo fibroblasts (REF52 cells) cell line was established by the group of W. Topp at Cold Spring Harbor Laboratory from 14-day rat embryo cells cultivated for 52 passages[42,43]. REF52 cells were cultured in Dulbecco's modified Eagle's medium (DMEM; 11965092, Invitrogen) containing 10% fetal bovine serum (FBS; 10082147, Invitrogen) and 1% penicillin/streptomycin (15070063, Invitrogen) at 37 °C in a 5% CO_2 humidified incubator. We authenticated REF52 cells as rat cells by immunolabelling proteins with rat-specific antibodies and knocking down genes with rat-specific SMARTpool siRNAs. Cells tested negative for mycoplasma by a PCR-based method[44], and mycoplasma-negative cells were stored and used in the experiments. Human endothelial HUVEC cells (ATCC, CRL-1730) were cultured in Medium 200 (M200500, Invitrogen) containing 10% large vessel endothelial supplement (LVES, A1460801, Invitrogen) and 1% gentamicin/amphotericin (R01510, Invitrogen) at 37 °C in a 5% CO_2 humidified incubator. Cells were transfected via electroporation using the Neon transfection system (MPK1096; Invitrogen) following the standard protocol. The following plasmids were used: F-Tractin-tdTomato (gift from M. J. Schell, Uniformed Services University, Bethesda, Maryland, USA); α-actinin-1-mCherry (gift from C. Otey, University of North Carolina, Chapel Hill, North Carolina, USA); α-actinin-4-mCherry (gift from M. Murata-Hori, The Institute for Stem Cell Biology and Regenerative Medicine, India); myosin regulatory light chain (RLC)-GFP[45] (gift from W. A. Wolf and R. L. Chisholm, Northwestern University, Chicago, Illinois, USA); myosin IIA heavy chain N terminal (MHC-IIA)-GFP[46,47] (gift from M. Sheetz, Mechanobiology Institute, Singapore); actin-mCherry (gift from C. M. Waterman, National Heart, Lung, and Blood Institute, NIH, Bethesda, Maryland, USA); GFP-Tropomodulin 3 (TMOD3) produced in our previous work[48].

siRNA knockdown. REF52 cells were transfected with ON-TARGETplus Rat siRNA SMARTpool library (Dharmacon) or a non-targeting control pool siRNA (D-001810-10-05, Dharmacon) at a concentration of 20 μM using electroporation (Neon, Invitrogen) according to the manufacturer's instructions. After 48 h, the cells were re-plated on 10 ng ml^{-1} fibronectin (11080938001, Roche)-coated glass coverslips (No. 1.5H, 017650, Marienfeld) and incubated for 16 h, before fixation and immunofluorescence staining for SIM imaging. siRNA sequences are available in Supplementary Table 1. Knockdowns of cofilin1 and α-actinin-4 were verified by western blotting using the antibodies anti-cofilin1 (Abcam, ab11062) and α-actinin-4 (Enzo Life Sciences, ALX-210-356), and rescued by expression of siRNA-resistant cofilin1-mCherry and α-actinin-4-mCherry, respectively.

Treatment with inhibitors. Addition and washout of inhibitors was performed directly under the microscope by pipetting carefully to obtain the same imaging field for each event. Each washout step was repeated three times quickly to remove the inhibitor completely. Live cell imaging of addition and then washout of the inhibitor of Rho kinase, Y27632 (Y0503, Sigma-Aldrich), was taken for Supplementary Video 15. Static images were taken for Fig. 4 and Supplementary Fig. 5. For the experiments presented in Fig. 4, 20 μM Y27632 was applied for 25 min firstly. Then, Y27632 was washed out and replaced with normal imaging culture medium alone or in the presence of 40 μM blebbistatin (13013-10, Cayman), or in the presence of a combination of 100 nM latrunculin A (L5163, Sigma-Aldrich) and 1 μM jasplakinolide (J4580, Sigma-Aldrich), or in the presence of 15 μM SMIFH2 (4401, TOCRIS). For the cells incubated with SMIFH2, an additional step of washout of SMIFH2 with normal imaging culture medium was added for 40 min. For the experiments presented in Supplementary Fig. 5, 40 μM blebbistatin (inhibition of myosin II contractility) was applied for 25 min to the control cells. For the treatment blocking actin dynamics, the combination of 1 μM jasplakinolide and 100 nM latrunculin A was applied for about 12 min to the control cells. For the treatment of formin inhibitor, 15 μM SMIFH2 was applied for 55 min to the control cells.

G-actin incorporation assay. The barbed ends are the fast-growing ends of the actin filaments and we visualized them as sites of incorporation of labelled G-actin. G-actin incorporation assay was slightly modified from that described previously[28,29]. G-actin conjugated with Alexa-Fluor 568 (A12374, Invitrogen) was diluted to 20 μM, and pretreated with sonication for 5 min followed by centrifuging for 3 min. Then 1 mM ATP was added to the G-actin-Alexa 568 solution for 5 min incubation. REF52 cells transfected with RLC-GFP or TMOD3-GFP were permeabilized with the permeabilization buffer M (50 mM imidazole, pH 6.8, 50 mM KC1, 0.5 mM $MgCl_2$, 0.1 mM EDTA, l mM EGTA, l mM 2-mercaptoethanol and 2 μl ml^{-1} protease inhibitors cocktail) supplemented with 0.003% digitonin and 0.4 μM G-actin-Alexa 568 for 5 min at room temperature. The cells were washed once with permeabilization buffer M; then the cells were fixed with 4% paraformaldehyde (PFA) for 15 min at room temperature, followed by three washes with 1× PBS. The fresh samples were ready for imaging.

Immunofluorescence antibody staining. Anti-myosin IIA tail domain (used as 1:1,000, M 8064) and anti-RLC (used as 1:400, M4401) were from Sigma-Aldrich; Alexa-Fluor 488-conjugated phalloidin (used as 1:1,000, A12379) and Alexa-Fluor-conjugated secondary antibodies (used as 1:400) were from Molecular Probes. Cells were fixed in warm 4% PFA for 15 min at 37 °C, washed with 1× PBS, permeabilized with 0.1% Triton X-100 (Sigma-Aldrich) for 5 min at room temperature, blocked with 1% bovine albumin serum (BSA; A7906, Sigma-Aldrich) for 1 h, immunofluorescence stained with primary antibodies overnight at 4 °C, and then incubated with secondary antibodies for 1 h at room temperature followed by three washes with 1× PBS.

Cell imaging using structured illumination microscopy (SIM) and FRAP-SIM experiments. To apply structured illumination microscopy (SIM), high-precision glass coverslips with thickness 170 μm (No. 1.5H, 017650, Marienfeld) were used as the substrate for cell plating. The glass coverslips were cleaned by overnight washing with 20% nitric acid, 10 washing with Milli-Q water afterwards, and followed by rinsing with absolute ethanol. Then the coverslips were air-dried in the clean hood. The cells were trypsinized and re-plated on 10 ng ml^{-1} fibronectin (11080938001, Roche)-coated glass coverslips for 2 h or 24 h. Before imaging, the coverslips were mounted onto the observation chamber (CM-B25-1 Chamlide CMB chamber) and changed to fresh imaging medium (Leibovitz's medium with 10% FBS and 1% penicillin–streptomycin).

Fixed cells and live cells were imaged by dual-colour 3D-SIM (Nikon), or epi-fluorescence light mounted in a SIM microscope (Supplementary Fig. 1a). The SIM images were taken with dual-colour (laser 488 and laser 561) SIM mode (based on full illumination, for imaging two fluorescent proteins simultaneously) using a 100× oil (NA 1.49) objective with autofocus maintained by the Nikon Perfect Focus system. The samples were mounted in a humidified cell culture chamber and maintained at 37 °C with 5% CO_2. The interval time between images is 30 s or 1 min for dual-colour SIM live cell imaging.

Figure 3a and Supplementary Videos 10, 16 and 17 were performed with dual-colour (laser 488 and laser 560) TIRF-SIM with high temporal resolution at the Advanced Imaging Center, HHMI Janelia Research Campus[49]. A 100× oil (NA 1.49) objective, and two cameras were used for dual-colour TIRF-SIM; the interval time between images is 10 s. The samples were mounted in a humidified cell culture chamber and maintained at 37 °C with 5% CO_2.

FRAP experiments were performed with 3D-SIM microscopy (Nikon). The bleaching set-up was controlled by using a photo activation laser with wavelength 488 nm (PA 488) or wavelength 561 nm (PA 561) with 15% power that is mounted in the N-SIM system. We took two sequential frames of the cell of interest before bleaching. Then a circular region (diameter 2 μm) in the middle of the observation view was bleached for 5 s without delay by using laser PA 488 or by both PA 488 and PA 561. Then recovery after bleaching was recorded for 5 or 6 min. During image acquisition, the time interval between frames was about 10 s for one-colour SIM mode (SIM 488) or 17 s for dual-colour SIM (SIM 488 and SIM 561).

Image analysis. For the measurements in Supplementary Fig. 2, the length and spacing between myosin II stacks were measured by line scanning of intensity profile in ImageJ/Fiji (http://rsb.info.nih.gov/ij), and the graph plotting and distribution analysis were performed using the technical graphing and data analysis software Igor Pro (WaveMetrics). To quantify the movement of myosin filament stacks in stress fibres or transverse arcs, we used particle image velocimetry (PIV) analysis. We applied MatPIV 1.6 (ref. 50), a free Matlab toolbox to calculate velocity maps. We used polar coordinates with cyan and purple arrows indicating the centripetal and centrifugal movements to plot the velocity arrows of movement of myosin stacks in transverse arcs of spreading cells. To show the different direction of myosin movement along stress fibres, we first rotated the image so stress fibres would be vertical. We used rectangular coordinates with cyan and purple arrows indicating upward and downward movements to plot the velocity of movement of myosin stacks in stress fibres. The line scan intensity profiles were generated using Igor Pro.

For the analysis of FRAP experiments, a region of interest (box) was manually selected such that it contained and followed only one bleached myosin stack, and we measured the average intensity of the boxed region over time in ImageJ/Fiji. The graph plotting and FRAP analysis were performed using Igor Pro. The graph of average intensity $I_{raw}(t)$ is displayed as the function of time t. To correct for the photobleaching effect by illumination with time, the average intensity of a reference region that is far away from the FRAP region is recorded with time, as $I_{ref}(t)$. The corrected intensity is calculated with the equation $I_{corr}(t) = (I_{raw}(t)/(I_{ref}(t)/I_{ref}(0)))$, where $I_{ref}(0)$ is the average intensity of a reference region at time 0. The graph of $I_{corr}(t)$ is plotted as a function of time. To fit with the standard FRAP equation, we normalized $I_{corr}(t)$ as $I_{nor}(t) = (I_{corr}(t) - I_{corr}(t_b)/I_{corr}(0) - I_{corr}(t_b))$, where t_b is the time immediately after bleaching and time 0 is the time of maximal fluorescence.

Then the graph of normalized intensity $I_{nor}(t)$ is fitted with the FRAP equation $I(t) = A - Ae^{-\tau t}$, for which the dissociation rate K_{off} is τ, the half-time is equal to $-ln0.5/\tau$ and the immobile fraction is equal to $1 - A$.

Statistics and reproducibility. Prism (GraphPad Software) was used for statistical analysis. The significance of the differences (P value) was calculated using two-tailed unpaired Student's t-test. The quantitative data are shown as mean ± s.d. The methods for statistical analysis and numbers of samples (n) were indicated in the figure legends.

The numbers of samples for the quantitative data are indicated in the figure legends. Images in Fig. 1a,c,d,f and Supplementary Fig. 1b,d,e are typical examples taken from a total of 15–35 images captured in more than three independent experiments. Fig. 1b,e and Supplementary Fig. 1a,c,f are typical representatives for more than 10 images taken in two independent experiments. The experiment shown in Fig. 2a was repeated four times, Fig. 2b was repeated five times and Fig. 2e three times and gave analogous results. Figure 3 shows the typical sequences observed in more than 15 cases in different experiments. Images in Fig. 4 and Supplementary Fig. 5 are representative for more than 6 independent experiments. Images in Fig. 5 are representative for more than 15 images from two independent experiments. Supplementary Fig. 3 and Supplementary Videos 3–6 are representative for the measurements performed for more than five different cells in each case.

Data availability. All data supporting the findings of this study are available from the corresponding author on request.

42. McClure, D. B., Hightower, M. J. & Topp, W. C. Effect of SV40 transformation on the growth factor requirements of the rat embryo cell line REF52 in serum-free medium. *Cold Spring Harb. Conf. Cell Prolif.* **9,** 345–364 (1982).
43. Matsumura, F., Lin, J. J., Yamashiro-Matsumura, S., Thomas, G. P. & Topp, W. C. Differential expression of tropomyosin forms in the microfilaments isolated from normal and transformed rat cultured cells. *J. Biol. Chem.* **258,** 13954–13964 (1983).
44. Goding, J. W. *Monoclonal Antibodies* 3rd edn, 181–183 (Academic, 1996).
45. Kengyel, A., Wolf, W. A., Chisholm, R. L. & Sellers, J. R. Nonmuscle myosin IIA with a GFP fused to the N-terminus of the regulatory light chain is regulated normally. *J. Muscle Res. Cell Motil.* **31,** 163–170 (2010).
46. Meshel, A. S., Wei, Q., Adelstein, R. S. & Sheetz, M. P. Basic mechanism of three-dimensional collagen fibre transport by fibroblasts. *Nat. Cell Biol.* **7,** 157–164 (2005).
47. Cai, Y. *et al.* Nonmuscle myosin IIA-dependent force inhibits cell spreading and drives F-actin flow. *Biophys. J.* **91,** 3907–3920 (2006).
48. Guo, Z. *et al.* E-cadherin interactome complexity and robustness resolved by quantitative proteomics. *Sci. Signal.* **7,** rs7 (2014).
49. Li, D. *et al.* Extended-resolution structured illumination imaging of endocytic and cytoskeletal dynamics. *Science* **349,** aab3500 (2015).
50. Sveen, J. K. *An Introduction to MatPIV v. 1.6.1* (Univ. Oslo, 2004).

Erratum: Long-range self-organization of cytoskeletal myosin II filament stacks

Shiqiong Hu, Kinjal Dasbiswas, Zhenhuan Guo, Yee-Han Tee, Visalatchi Thiagarajan, Pascal Hersen, Teng-Leong Chew, Samuel A. Safran, Ronen Zaidel-Bar and Alexander D. Bershadsky

Nature Cell Biology **19,** 133–141 (2017); published online 23 January 2017; corrected after print 31 January 2017

In the version of this Letter originally published, the numbering of Supplementary Video files and the references to those files in the text did not match. All online versions of the Letter have been corrected so that the Supplementary Videos are numbered sequentially from 1–17.

nature cell biology

DOI: 10.1038/ncb3466

In the format provided by the authors and unedited.

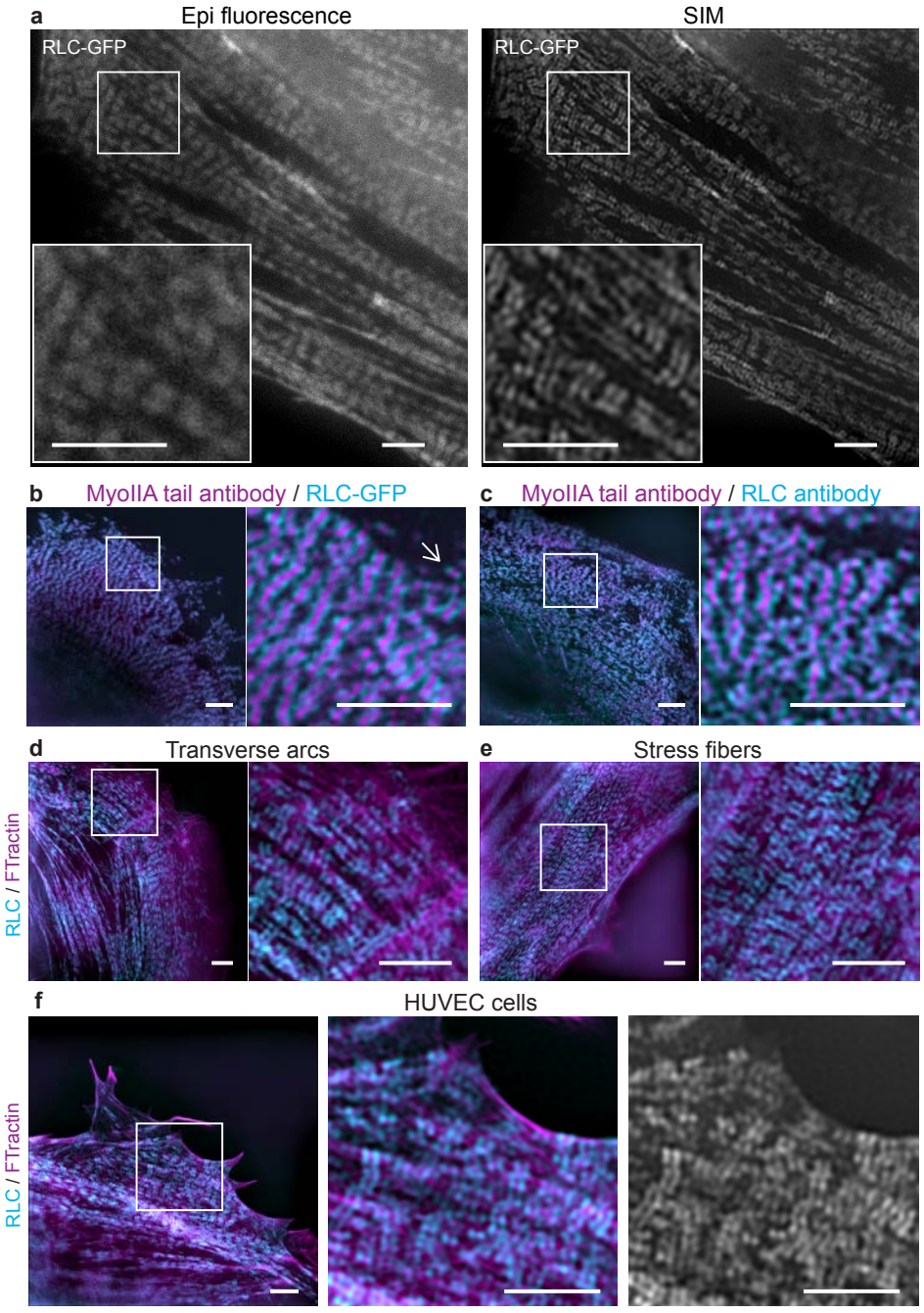

Supplementary Figure 1 Structured illumination microscopy (SIM) reveals the organization of myosin-IIA filaments in non-muscle cells. (a) EPI fluorescence (left) and SIM (right) images showing localization of RLC-GFP in the same region of REF52 cells. Boxed parts are shown at high magnification in the corresponding insets. (b) RLC-GFP (cyan) labelled REF52 cells fixed and stained with an antibody to the C-terminal end of the myosin-IIA heavy chain (myosin-IIA tails, magenta). Left panel: low magnification merged image; right panel: high magnification of the boxed area. Note that myosin-IIA tails (magenta) are localized to the space between the myosin heads decorated by RLC-GFP (cyan). (c) Double immunofluorescence staining of endogenous myosin light chain (RLC, cyan) and myosin-IIA tails (magenta). Left panel: low magnification merged image; right panel: high magnification of the boxed area. The pattern of myosin-II organization is similar to that in cells transfected with exogenous RLC-GFP shown in b. (d) The distribution of myosin stacks along transverse arcs in REF52 cells. The cells express RLC-GFP (cyan) and F-Tractin-tdTomato (magenta). The boxed area was shown at high magnification in the right panel. (e) The distribution of myosin stacks along stress fibers in REF52 cells. The cells express RLC-GFP (cyan) and F-Tractin-tdTomato (magenta). The boxed area is shown at high magnification in the right panel. Note that myosin stacks are oriented orthogonal to actin bundles both in arcs and stress fibers. The spacing between neighboring stacks is larger in arcs than in stress fibers (see quantitative data in Supplementary Figures 2 g-i). (f) Visualization of myosin-II stack organization in human endothelial HUVEC cells. The cells express RLC-GFP (cyan) and F-Tractin-tdTomato (magenta). Left panel: low magnification merged image; middle and right panel show high magnification of merged image and RLC image for the boxed area, respectively. The SIM microscopy was performed using Nikon 3D-SIM. Scale bars, 3 μm.

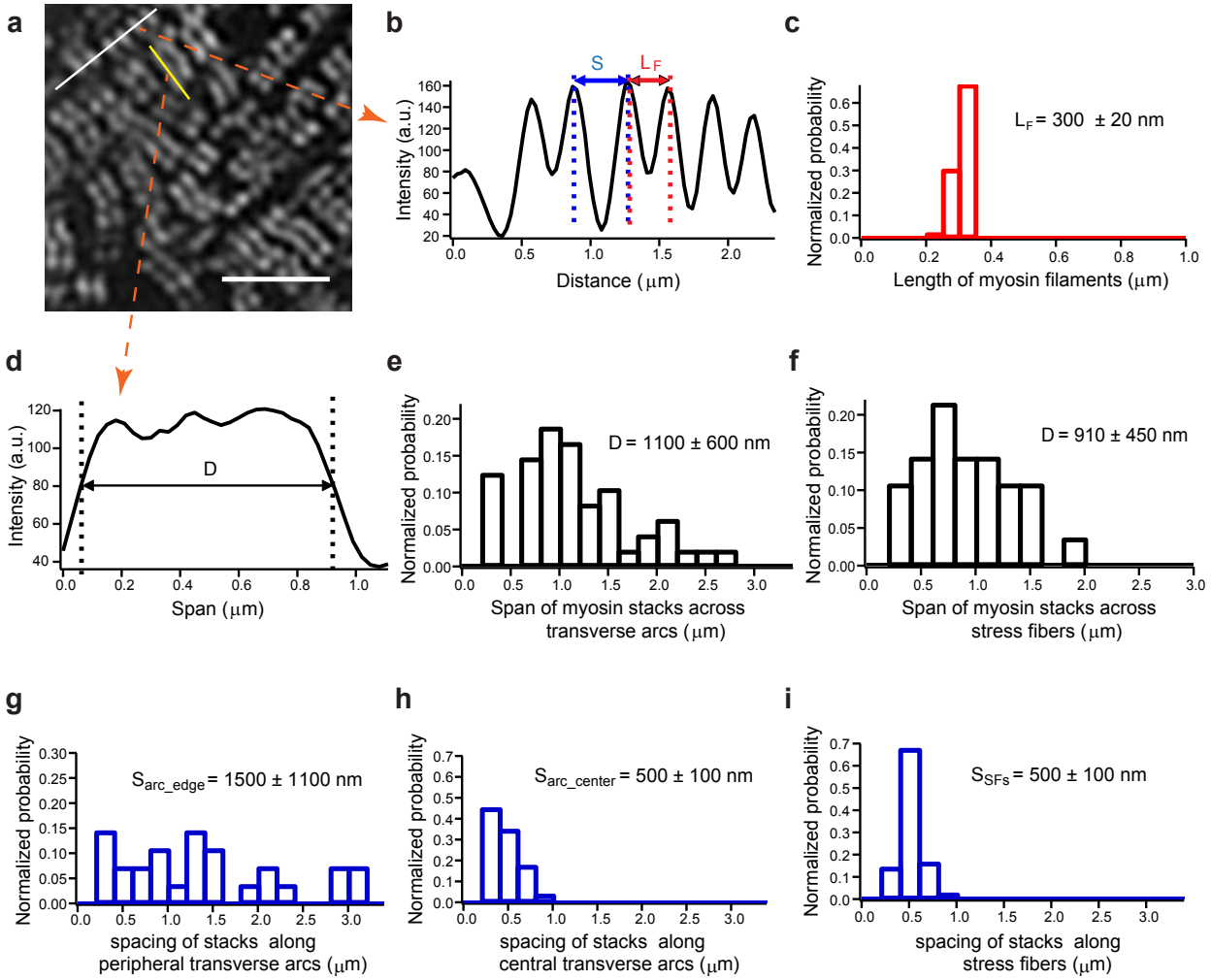

Supplementary Figure 2 Quantitative characteristics of myosin-II stack distribution along transverse arcs and stress fibers. (a) Myosin-II stacks shown by labelling with RLC-GFP were line scanned in a perpendicular direction (corresponding to direction of actin bundles) as shown by the white line or along the direction of stack as shown by the yellow line. The results of the intensity measurements are shown in (b) and (d), respectively. The length of individual myosin filaments (L_F) and spacing between them (S) were defined as indicated on graph (b); the span of myosin stacks were defined as on graph (d). (c) Distribution of the individual myosin filaments length (the distance between peaks corresponding to myosin head labelling by RLC-GFP) (n = 53 filaments from 6 cells). (e and f) Distribution of the span of myosin-IIA stacks associated with transverse arcs (n = 28 filaments from 3 cells, (e)) and stress fibers (n = 48 filaments from 3 cells, (f)). In both cases, the myosin-II stacks were oriented orthogonal to the direction of the associated actin bundles. Note that while average span of myosin-II stacks associated with stress fibers is slightly lower than that of the stacks associated with transverse arcs, the difference is not significant (p=0.0657 by two-tailed unpaired student's t-test). (g-i) Distribution of spacing between neighboring myosin-II stacks along peripheral transverse arcs (n = 28 filaments from 3 cells, (g)), centrally located arcs (n = 29 filaments from 3 cells, (h)), and stress fibers (n = 43 filaments from3 cells, (i)). Note that spacing between myosin stacks in stress fibers (i) is uniform, while the spacing between the stacks along transverse arcs varied in a broad range, being wider at the cell periphery (g) and narrower in the central part of the cell (h). There is significant difference between (g) and (h) (P<0.0001, by two-tailed unpaired student's t-test); however there is no significant difference between (h) and (i) (p=0.2954, by two-tailed unpaired student's t-test). The results of measurements indicated in the figure are all presented in the form "mean ± SD". Scale bar, 2 μm.

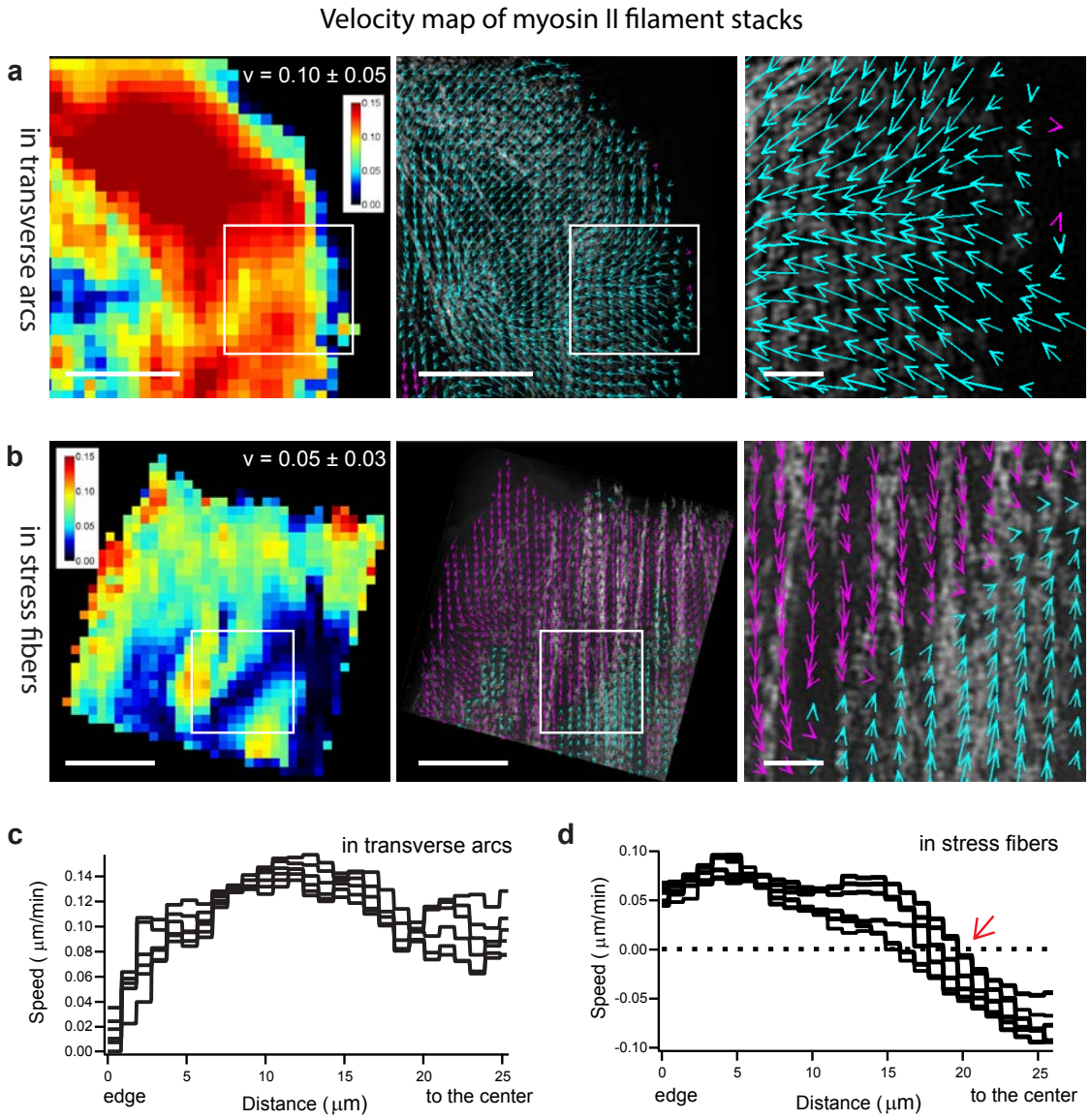

Supplementary Figure 3 The comparison of myosin stacks movement in transverse arcs and stress fibers. Quantification of the movement of myosin stacks in transverse arcs (see Supplementary Videos 3, 4) and stress fibers (see Supplementary Videos 5, 6) using particle image velocimetry analysis is presented in figures (a) and (b), respectively. The fields of the myosin stack velocities were obtained by averaging the instant velocities during the period of observation. For the transverse arcs (a), we used a polar system of coordinates with cyan and magenta arrows symbolizing the centripetal and centrifugal movements, respectively. The magnitudes of the movement velocities are represented by "spectral" color coding in the left image (the mean velocities±SD values are shown above) and by arrow length in the middle and right images. The boxed area is shown at high magnification in the right image. For the parallel stress fibers (b), we used a rectangular system of coordinates with one axis oriented along the direction of the stress fibers. Left image shows the distribution of stacks velocities in "spectral" color coding. In the middle and right images, cyan and magenta arrows denote the myosin stacks movement in positive (from bottom to top of the image) and negative (from top to bottom) direction, respectively. Note that the movement of myosin stacks along the stress fibers is oriented from the fiber ends at the periphery of the cell, but changed the signs in the central zone of the stress fibers. The boxed area is shown at high magnification in the right image. Graphs in (c) and (d) show velocities of the centripetal movement of the myosin-II stacks along transverse arcs and stress fibers, respectively. The movement of stacks associated with transverse arcs was always retrograde and its rate increased with the distance from the cell edge approaching a plateau in the central part of the cell (c). Note that at some distance from the cell edge, the sign of the velocity of the stack movement along the stress fibers changed (arrow) showing the transition from retrograde to anterograde movement (d). Scale bars: 10 μm (left and center), 2 μm (right).

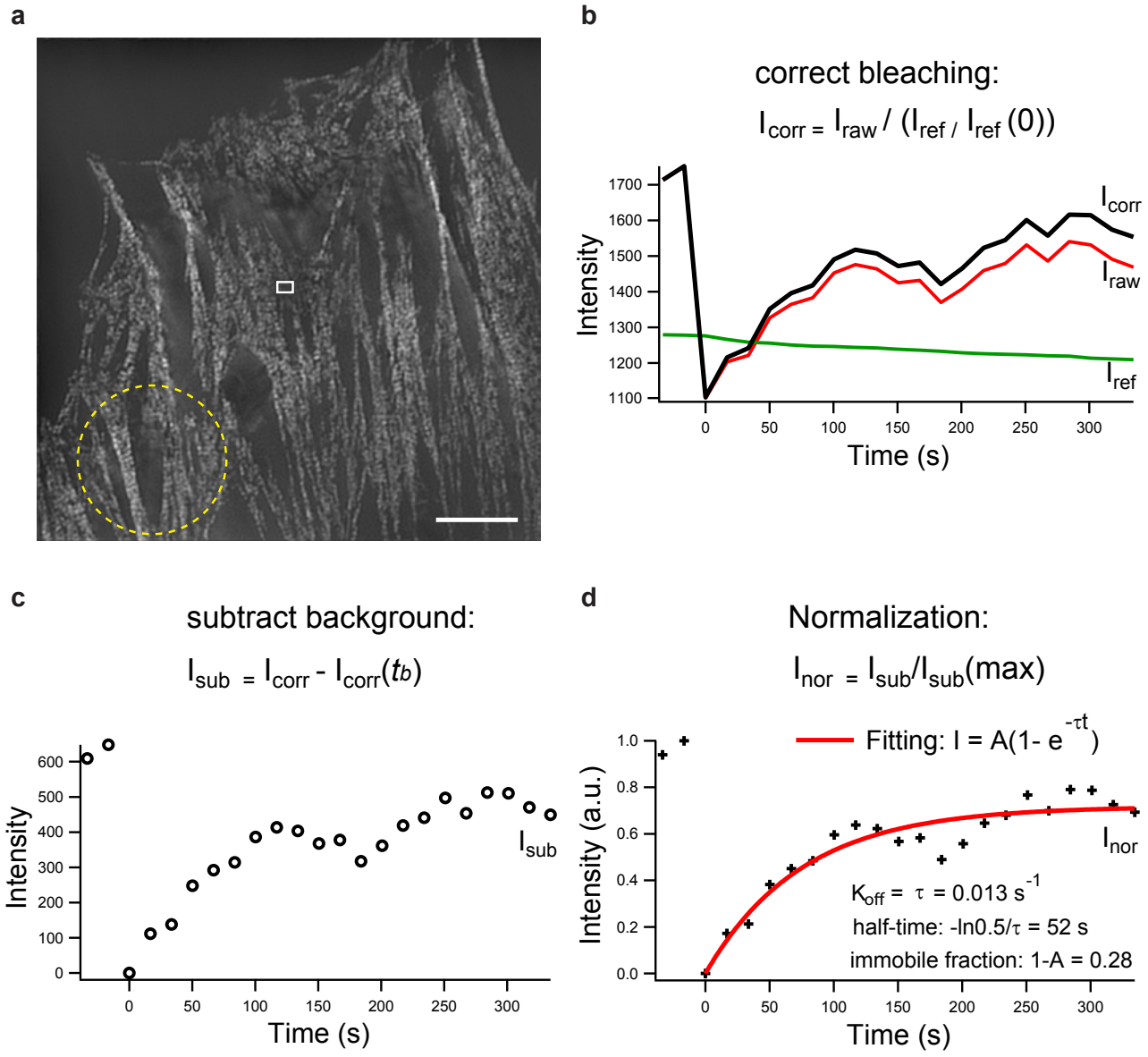

Supplementary Figure 4 The workflow of FRAP experiment analysis. (a) The bleached myosin stack (MHC-IIA-GFP, white box) was detected and followed as a function of time, average intensity as $I_{raw}(t)$; a region far away from bleached area was chosen as a reference region (yellow circle), average intensity of reference region is $I_{ref}(t)$. (b) To correct photo-bleaching effect of illumination, the intensity was corrected as $I_{corr}(t)=I_{raw}(t)/(I_{ref}(t)/I_{ref}(0))$. (c) The background was subtracted by setting the minimal intensity as 0. Thus background subtracted intensity $I_{sub}(t)= I_{corr}(t)- I_{corr}(t_b)$, where t_b is the time immediately after bleaching. (d) To fit with standard FRAP equation, the maximal intensity was set as 1, and the graph was normalized to 0 – 1 interval. The graph was fitted to the exponential equation $I(t)=A-Ae^{-\tau t}$. The parameters K_{off}, half-time and immobile fraction were calculated as shown in the figure. FRAP experiments were performed using Nikon 3D-SIM. Scale bar, 5μm.

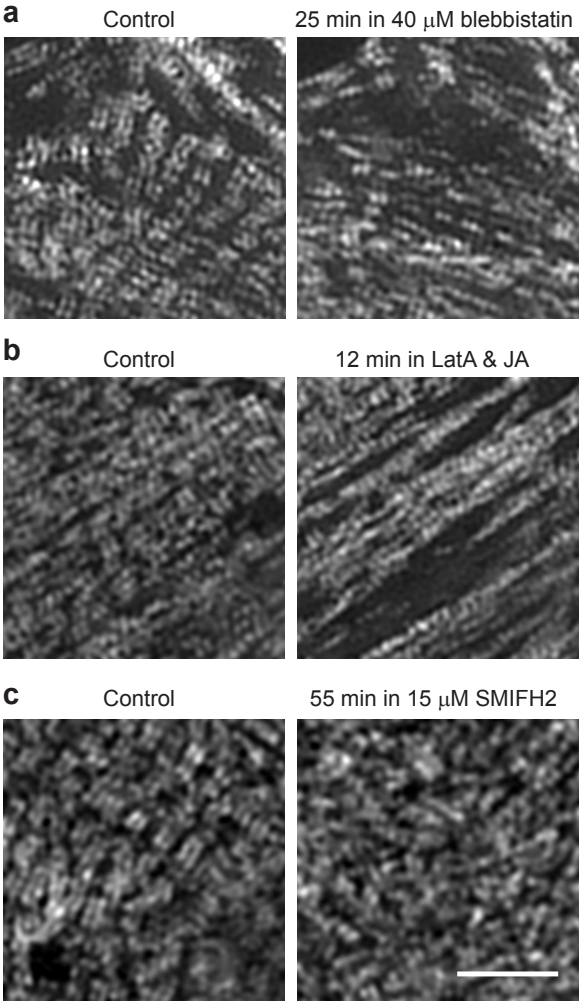

Supplementary Figure 5 Myosin ATPase activity and actin filament dynamics are required for myosin-II stack maintenance. (a) Myosin-II labelled with RLC-GFP before (left column) and after 25 minutes incubation with 40 μM blebbistatin (right column). Note that the numerous myosin filaments are preserved, while the stacks of myosin filaments are significantly disintegrated. (b) Treatment of cells with a mixture of latrunculin-A (LatA) and jasplakinolide (JA) led to disruption of the myosin stack organization. Such treatment was previously shown to suppress actin filament dynamics (Fig. 2f,g). Note that myosin stacks are significantly disrupted after 12 minutes of treatment with 100 nM latrunculin-A and 1 μM jasplakinolide. (c) Myosin-II (labelled with RLC-GFP) in the cell treated with an inhibitor of formins, 15 μM SMIFH2 for 55 minutes. Note that numerous individual myosin filaments are intact, while stack organization of the myosin filaments is significantly suppressed. The experiments were performed using Nikon 3D-SIM. Scale bar, 3 μm, is same for all the images.

Supplementary Table Legends

Supplementary Table 1 Sequences of siRNAs used in the study.

Supplementary Video Legends

Supplementary Video 1 Dynamics of myosin-II and α-actinin in REF52 cells. Myosin-II and α-actinin were labelled by expression of RLC-GFP (green) and α-actinin-mCherry (red), respectively. The transfected cells were filmed two hours after replating for 30 minutes with 30 second intervals between frames using Nikon dual color 3D-SIM. The scale bar is 5 μm. The display rate is 30 fps.

Supplementary Video 2 Visualization of the actin filaments pointed ends by labeling with GFP-tropmodulin 3. The cells were co-transfected with GFP-tropmodulin 3 (GFP-TMOD3, cyan) and α-actinin-mCherry (red) and filmed two hours after replating for 60 minutes with 1 minute intervals between frames using Nikon dual color 3D-SIM. The scale bar is 5 μm. The display rate is 15 fps.

Supplementary Video 3 Dynamics of myosin-II filaments and F-actin in transverse arcs of a spreading cell. Dynamics of myosin-II (left) and F-actin (right) in the same field were visualized by expressing RLC-GFP and F-Tractin-tdTomato. Cell was filmed two hours after replating for 30 minutes with 1 minute intervals between frames with Nikon dual color 3D-SIM. The scale bar is 5 μm. The display rate is 15 fps. Notice that myosin stacks move centripetally together with actin transverse arcs.

Supplementary Video 4 PIV analysis of myosin-II filament movements in transverse arcs. Particle image velocimetry (PIV) analysis of the movements of myosin-II filament stacks shown in Supplementary Video 3 left was performed using Matlab toolbox. Velocity maps (cyan and purple arrows symbolizing the centripetal and centrifugal movements, respectively, while arrow lengths are proportional to the velocity) were calculated for each frame. The video showing the evolution of velocity distribution is merged with the images of myosin stacks (Supplementary Video 3 left). The interval between frames was 1 minute and duration of entire video was 30 minutes. The display rate is 15 fps.

Supplementary Video 5 Dynamics of myosin-II filament stacks and F-actin in stress fibers. Dynamics of myosin-II (left) and F-actin (right) in the same field were visualized by expressing RLC-GFP and F-Tractin-tdTomato. Cell was filmed 24 hours after replating for 60 minutes with 1 minute intervals between frames with Nikon dual color 3D-SIM. The scale bar is 5 μm. The display rate is 15 fps.

Supplementary Video 6 PIV analysis of myosin-II filament movements in stress fibers. Results of the PIV analysis of the Supplementary Video 5 left are shown. Cyan and purple arrows denoted the particle movements in positive (from bottom to top of the image) and negative (from top to bottom) direction, respectively, while arrow lengths are proportional to the velocity. Velocity maps were calculated for each frame. The video showing the evolution of velocity distribution is merged with the images of myosin stacks (Supplementary Video 5 left). The interval between frames was 1 minute and duration of entire video was 60 minutes. The display rate is 15 fps.

Supplementary Video 7 FRAP-SIM of myosin light chain-GFP. FRAP experiment on myosin light chain GFP (RLC-GFP) was performed with Nikon 3D-SIM. 2 frames with interval of 10 seconds were taken before bleaching, followed by 5 seconds of bleaching in a circular region (diameter 2 μm) in the middle of observation view. 31 frames with 10 second intervals were taken after bleaching. The myosin stack of interest is framed in a box. The scale bar is 5 μm. The display rate is 5 fps.

Supplementary Video 8 FRAP-SIM on myosin heavy chain-GFP and actin-mCherry. FRAP experiment of MHC-IIA GFP (left) and actin-mCherry (right) were performed with Nikon 3D-SIM. 2 frames with interval of 17 seconds were taken before bleaching, followed by 5 seconds of bleaching, and 21 frames with 17 second intervals after bleaching. The myosin stack of interest (boxed) was located inside the circular bleached zone with diameter 2 μm. The corresponding box was indicated in the actin image (right).The scale bar is 3 μm. The display rate is 5 fps.

Supplementary Video 9 FRAP-SIM on myosin heavy chain-GFP and actin-mCherry in condition of actin filament stabilization. FRAP experiment of MHC-IIA GFP (left) and actin-mCherry (right) was performed immediately after addition of 100 nM latrunculin A and 1 μM jasplakinolide. 2 frames with interval of 17 seconds were taken before bleaching, followed by 5 seconds of bleaching, and 21 frames with 17 second intervals after bleaching. The myosin stack of interest (boxed) was located inside the circular bleached zone with diameter 2 μm. The corresponding box was indicated in the actin image (right). Note that fluorescence of actin was not recovered under these conditions, while fluorescence of MHC-IIA filament stack did recover. The scale bar is 3 μm. The display rate is 5 fps.

Supplementary Video 10 Individual myosin filaments moving towards each other to form a stack. Cells expressing myosin light chain (RLC-GFP) were filmed for 30 minutes with 10 second intervals using TIRF-SIM (AIC, Janelia Research Campus). This 120 seconds fragment was taken 18 minutes after washout of Y27632 when the system of myosin-II stacks was essentially recovered. The scale bar is 1 μm. The display rate is 5 fps.

Supplementary Video 11 Formation of stacks between myosin filaments associated with actin bundles is accompanied by merging of these bundles. Cells co-expressing myosin light chain (RLC-GFP, green) and F-Tractin-tdTomato (red) were filmed for 14 minutes with 1 minute intervals using Nikon dual color 3D-SIM. The scale bar is 1 μm. The display rate is 5 fps. The movements of myosin filaments were shown in the central panel, dynamics of F-actin in the same field - in the right panel, and merged images - in the left panel. The arrows indicated myosin filaments associated with thin actin bundle that are moving towards other myosin filaments (or filament stacks) associated with a thicker actin bundle and finally joining them forming larger stacks. As a result, the thin actin bundle associated with these filaments moved and merged with thicker actin bundle.

Supplementary Video 12 Formation of stacks between myosin filaments associated with actin bundles is accompanied by merging of these bundles. Cells co-expressing myosin light chain (RLC-GFP, green) and F-Tractin-tdTomato (red) were filmed for 14 minutes with 1 minute intervals using Nikon dual color 3D-SIM. The scale bar is 1 μm. The display rate is 5 fps. The movements of myosin filaments were shown in the central panel, dynamics of F-actin in the same field - in the right panel, and merged images - in the left panel. The arrows indicated myosin filaments associated with thin actin bundle that are moving towards other myosin filaments (or filament stacks) associated with a thicker actin bundle and finally joining them forming larger stacks. As a result, the thin actin bundle associated with these filaments moved and merged with thicker actin bundle.

Supplementary Video 13 The alignment of two myosin filament stacks leading to formation of a larger new stack. Cells co-expressing myosin light chain (RLC-GFP, green) and FTractin-tdTomato (red) were filmed for 8 minutes with 2 minute intervals using Nikon dual color 3D-SIM. The scale bar is 1 μm. The display rate is 2 fps. The movements of myosin stacks are shown in the central panel, dynamics of F-actin in the same field - in the right panel, and merged images - in the left panel. Note that two myosin stacks indicated by arrows aligned with each other forming one single stack.

Supplementary Video 14 Individual myosin filaments travelling for a long distance before joining a pre-existing myosin filament stack. Cells co-expressing myosin light chain (RLC-GFP, green) and α-actinin-mCherry (red) were filmed for 16 minute with 30 second intervals using Nikon dual color 3D-SIM. The scale bar is 1 μm. The display rate is 5 fps. The movements of myosin filaments are shown in the central panel, dynamics of α-actinin in the same field - in the right panel, and merged images - in the left panel. Note that myosin filament indicated by arrow moved directionally for several microns before joining the pre-existing filament stack.

Supplementary Video 15 Rho kinase inhibitor Y27632 disrupted myosin-II filaments and filament stacks, while its washout led to complete recovery of the myosin-II filament stacks organization. Cells expressing myosin light chain (RLC-GFP, green) were filmed for total time of 115 minutes with 30 second intervals using Nikon 3D-SIM, beginning with 30 minutes in normal culture medium, followed by 35 minutes in the presence of 20 μM of Y27632, and ending by 50 minutes in fresh medium after washout of Y27632. The scale bar is 5 μm. The display rate is 30 fps.

Supplementary Video 16 Disruption of actin bundles and appearance of intervening network upon Y27632 treatment. REF52 cells expressing F-Tractin-tdTomato were filmed for 3.5 minutes during Y27632 treatment with 10 second intervals using TIRF-SIM (AIC, Janelia Research Campus). Actin organization changed from dense parallel bundles to sparse bundles interconnected with a network of thin, curvy fibers. The scale bar is 5 μm. The display rate is 15 fps.

Supplementary Video 17 Recovery of parallel actin bundles upon washout of Y27632. The same cell as in Supplementary Video 16 was filmed for 23 minutes during washout of Y27632 with 10 second intervals using TIRF-SIM (AIC, Janelia Research Campus). The disordered intervening actin network eventually organized into parallel actin bundles upon recovery. The scale bar is 5 μm. The display rate is 15 fps.